Development of an optimized backbone of FRET biosensors for kinases and GTPases

Naoki Komatsu[a], Kazuhiro Aoki[a,b], Masashi Yamada[c], Hiroko Yukinaga[c], Yoshihisa Fujita[c], Yuji Kamioka[c,d], and Michiyuki Matsuda[a,c]

[a]Laboratory of Bioimaging and Cell Signaling, Graduate School of Biostudies, Kyoto University, Kyoto 606-8501, Japan; [b]PREST, Japan Science and Technology Agency (JST), Saitama 332-0012, Japan; [c]Department of Pathology and Biology of Diseases, Graduate School of Medicine, and [d]Innovative Techno-Hub for Integrated Medical Bio-Imaging, Kyoto University, Kyoto 606-8501, Japan

ABSTRACT **Biosensors based on the principle of Förster (or fluorescence) resonance energy transfer (FRET) have shed new light on the spatiotemporal dynamics of signaling molecules. Among them, intramolecular FRET biosensors have been increasingly used due to their high sensitivity and user-friendliness. Time-consuming optimizations by trial and error, however, obstructed the development of intramolecular FRET biosensors. Here we report an optimized backbone for rapid development of highly sensitive intramolecular FRET biosensors. The key concept is to exclude the "orientation-dependent" FRET and to render the biosensors completely "distance-dependent" with a long, flexible linker. We optimized a pair of fluorescent proteins for distance-dependent biosensors, and then developed a long, flexible linker ranging from 116 to 244 amino acids in length, which reduced the basal FRET signal and thereby increased the gain of the FRET biosensors. Computational simulations provided insight into the mechanisms by which this optimized system was the rational strategy for intramolecular FRET biosensors. With this backbone system, we improved previously reported FRET biosensors of PKA, ERK, JNK, EGFR/Abl, Ras, and Rac1. Furthermore, this backbone enabled us to develop novel FRET biosensors for several kinases of RSK, S6K, Akt, and PKC and to perform quantitative evaluation of kinase inhibitors in living cells.**

Monitoring Editor
Karsten Weis
University of California, Berkeley

Received: Jan 26, 2011
Revised: Sep 7, 2011
Accepted: Sep 26, 2011

INTRODUCTION

Förster (or fluorescence) resonance energy transfer (FRET) is a process of nonradiative energy transfer between donor and acceptor fluorophores (Jares-Erijman and Jovin, 2003). This process depends on the proper spectral overlap of the donor emission and acceptor excitation, the distance between them, and the relative orientation of the fluorophore's transition dipole moments (Miyawaki, 2003). With the advent of a myriad of fluorescent proteins (FPs), genetically encoded biosensors based on FRET (hereafter referred to as FRET biosensors) have been increasingly used to visualize the activities of cellular signaling molecules such as Ca^{2+}, phospholipids, small GTPases, protein kinases, and so forth (Miyawaki, 2003; Aoki *et al.*, 2008). These FRET biosensors have contributed to our understanding of the spatiotemporal dynamics of signaling molecules in living cells, which could not be adequately investigated using the techniques of conventional biochemistry.

The genetically encoded FRET biosensors are classified into two types: intramolecular (or unimolecular) FRET biosensors and intermolecular (or bimolecular) FRET biosensors (Miyawaki, 2003). The former contain both donor and acceptor FPs within a single biosensor, whereas the latter consist of a pair of molecules conjugated with a donor FP and an acceptor FP, respectively. To date, intramolecular FRET biosensors have been widely used in cell biology due to the following advantages: high signal-to-noise ratio, easy loading of the biosensor into the cells, and simple ratiometric image analysis (Miyawaki, 2003; Aoki *et al.*, 2008).

This article was published online ahead of print in MBoC in Press (http://www.molbiolcell.org/cgi/doi/10.1091/mbc.E11-01-0072) on October 5, 2011.

The authors declare competing financial interest: M.M. filed a patent application for the reported linker: Japan patent application, 2010.

Address correspondence to: Kazuhiro Aoki (k-aoki@lif.kyoto-u.ac.jp).

Abbreviations used: CFP, cyan fluorescent protein; cp, circularly permutated; dbcAMP, dibutyryl-cyclical AMP; ECFP, enhanced CFP; Eevee, extension for enhanced visualization by evading extraFRET; FP, fluorescent protein; FRET, Förster (or fluorescence) resonance energy transfer; GAP, GTPase-activating protein; PH, Pleckstrin homology, TFP, teal fluorescent protein; TPA, tetradecanoylphorbol 13-acetate; YFP, yellow fluorescent protein.

© 2011 Komatsu *et al*. This article is distributed by The American Society for Cell Biology under license from the author(s). Two months after publication it is available to the public under an Attribution–Noncommercial–Share Alike 3.0 Unported Creative Commons License (http://creativecommons.org/licenses/by-nc-sa/3.0).

"ASCB®," "The American Society for Cell Biology®," and "Molecular Biology of the Cell®" are registered trademarks of The American Society of Cell Biology.

A serious disadvantage of the intramolecular FRET biosensors is that it is difficult to render them highly sensitive. Although several research groups have generated a number of FP variants that are optimized for FRET applications (Karasawa *et al.*, 2004; Rizzo *et al.*, 2004; Nguyen and Daugherty, 2005), the development of FP pairs for FRET is still one of the greatest challenges in FRET biosensor development (Li *et al.*, 2006). Even if we could choose optimal FP pairs, there would remain the harder task of designing the composition of domains to be included in the biosensors. The FRET efficiency of intramolecular biosensors is influenced primarily by the distance and the relative orientation of the two fluorophores (Jares-Erijman and Jovin, 2003; Nagai *et al.*, 2004). Because these two parameters are hard to predict, the developers are forced to spend large amounts of time in optimizing the biosensors by trial and error.

To circumvent these problems, we exploited an optimized backbone of intramolecular FRET biosensors. We first optimized the FPs and then developed a long, flexible linker that markedly increased the gain of FRET signals. This new backbone enabled us to improve the previously reported FRET biosensors of PKA, ERK, JNK, EGFR/Abl, Ras, and Rac1 and to develop new FRET biosensors for RSK, S6K, Akt, and PKC Ser/Thr kinases in a short period of time. Furthermore, by using cells stably expressing a FRET biosensor, we quantitatively and rapidly evaluated the effect of several kinase inhibitors on ERK activity.

RESULTS

Strategy for rational design of intramolecular FRET biosensors

To accelerate the development of the intramolecular FRET biosensors, we attempted to provide an optimized backbone structure. The prototype FRET biosensor used in this study comprises 1) a sensor domain and a ligand domain connected by a flexible linker, and 2) cyan and yellow FPs (CFP and YFP) serving as a donor and an acceptor, respectively (Figure 1A). The sensor domain changes its conformation upon perception of the signal. This sensitized sensor domain interacts with the ligand domain, thereby inducing a global change of the biosensor conformation and concomitant increase (or decrease in some cases) of the FRET efficiency from the donor to the acceptor.

The FRET efficiency of the intramolecular FRET biosensor is dependent primarily on the distance and the relative orientation of the donor and the acceptor (Miyawaki, 2003). Although the "orientation-dependent" FRET biosensor may be able to exhibit higher sensitivity than does the "distance-dependent" FRET biosensor (Jares-Erijman and Jovin, 2003), we could hardly predict and control the orientation of the donor and the acceptor for the development of an optimal FRET biosensor because we usually do not know the three-dimensional structures of the biosensor of which the sensor domain is bound ("ON") and not bound ("OFF") to the ligand domain. Thus the main job of our intramolecular FRET biosensors is to eliminate the orientation-dependent FRET and to render the biosensors completely distance-dependent with a long, flexible linker.

Before the evaluation of FRET biosensors described in this study, we will define the technical terms related to their performance. In the present FRET biosensors, the CFP and YFP variants are mostly used as the donor and the acceptor, respectively; therefore we will describe CFP and YFP as the default donor and the acceptor, respectively. FRET is detected by ratiometry (Jares-Erijman and Jovin, 2003): Cells are excited at a 440 nm wavelength, and the ratio of fluorescence intensity of the YFP channel (FRET) versus fluorescence intensity of the CFP channel (CFP), FRET/CFP, is used to represent the level of FRET ON state. Here, the "dynamic range" of the FRET biosensor is the theoretical range of FRET/CFP in the ON state biosensor and that in the OFF state (Figure 1C). In practical use, the change of activity or concentration of the molecule is monitored by the change of FRET/CFP after stimulation. This "gain" of the FRET signal is the relative increase or decrease in FRET/CFP after stimulation and is expressed as a percentage of the FRET/CFP value before stimulation. Therefore the gain of a FRET biosensor expressed in a certain cell type depends on both the dynamic range of the FRET biosensor and the increase in the fraction of the ON state after stimulation versus that before stimulation (Figure 1C). Meanwhile, "sensitivity" of FRET biosensors denotes a concentration of stimulants that increases the FRET/CFP value to 50% of the dynamic range (Figure 1C).

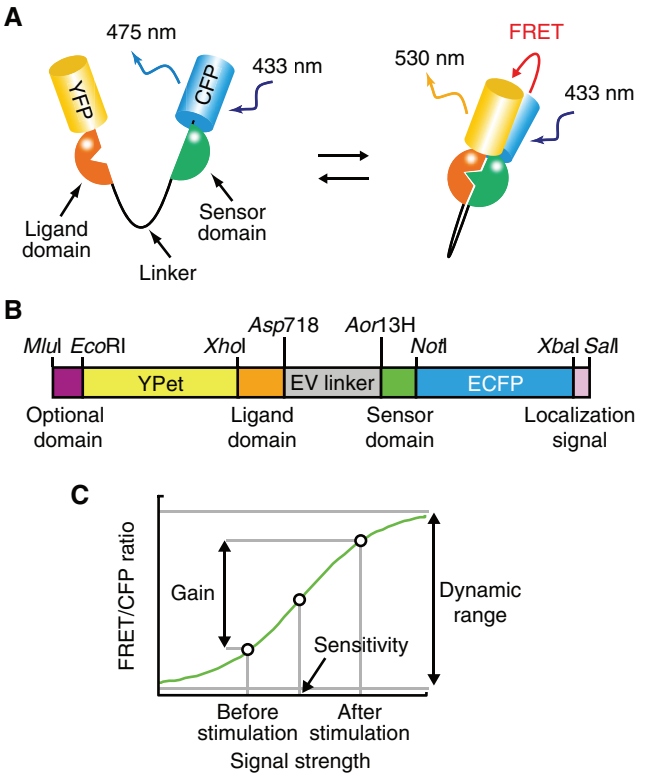

FIGURE 1: Optimized backbone of an intramolecular FRET biosensor. (A) Mode of action of the intramolecular FRET biosensor. (B) Structure of the DNA encoding an optimized intramolecular FRET biosensor. Shown are the unique restriction enzyme sites used to exchange each domain for the development of the biosensor. (C) Schematic representation of the titration curve of FRET/CFP ratio in intramolecular FRET biosensors.

Optimization of FRET donor and acceptor pairs

We first optimized the donor and acceptor FPs in the distance-dependent intramolecular FRET biosensor. The prototype biosensor is based on the structure of a PKA activity sensor, AKAR3 (Allen and Zhang, 2006), which contained a consensus peptide of PKA phosphorylation (Zhang *et al.*, 2001) and the phosphate binding domain of FHA1 (Figure 2A). We initially used a 72-amino-acid (a.a.) polyglycine linker used in an ERK activity sensor, EKAR, as a flexible long linker (Harvey *et al.*, 2008). We tested teal fluorescent protein (TFP)- and CFP-derived FPs, including enhanced CFP (ECFP), Turquoise-GL, and CyPet, as donor FPs, and we examined YFP-derived FPs, including Venus, circularly permutated Venus mutants, mCitrine, and YPet (see *Materials and Methods* and Supplemental Table S1), as acceptor FPs. The gain of the biosensors was quantified in HeLa

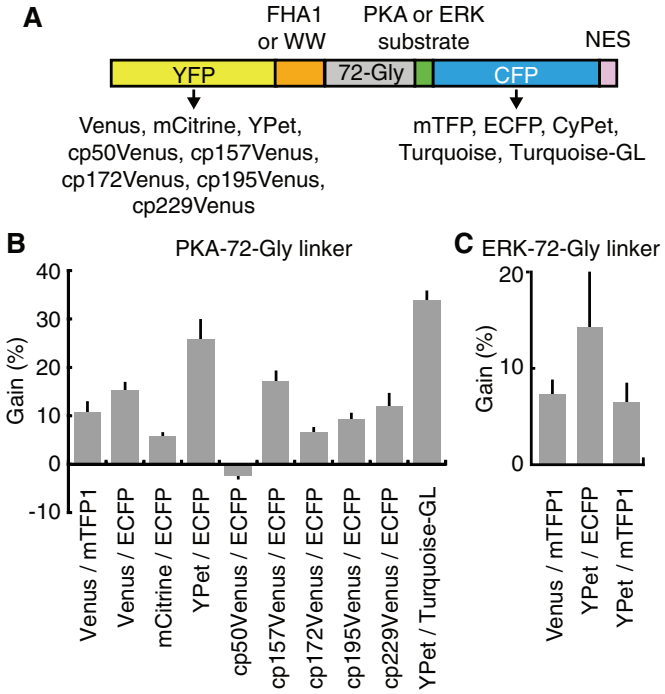

FIGURE 2: Optimization of pairs of FPs for distance-dependent FRET biosensors. (A) Scheme of the PKA or ERK activity sensor consisting of YFPs (donor), a FHA1 or WW phosphopeptide binding domain (ligand domain), a 72-Gly linker, a PKA or ERK substrate (sensor domain), CFPs (acceptor), and nuclear export signal (NES). (B) HeLa cells expressing AKAR3 with various pairs of FPs as indicated were stimulated with 1 mM dbcAMP for 10 min. The gain in FRET/CFP is represented with the SD (n > 5). (C) HeLa cells expressing EKAR with various pairs of FPs as indicated were stimulated with 10 ng/ml EGF for 10 min. The gain in FRET/CFP is represented with the SD (n > 5).

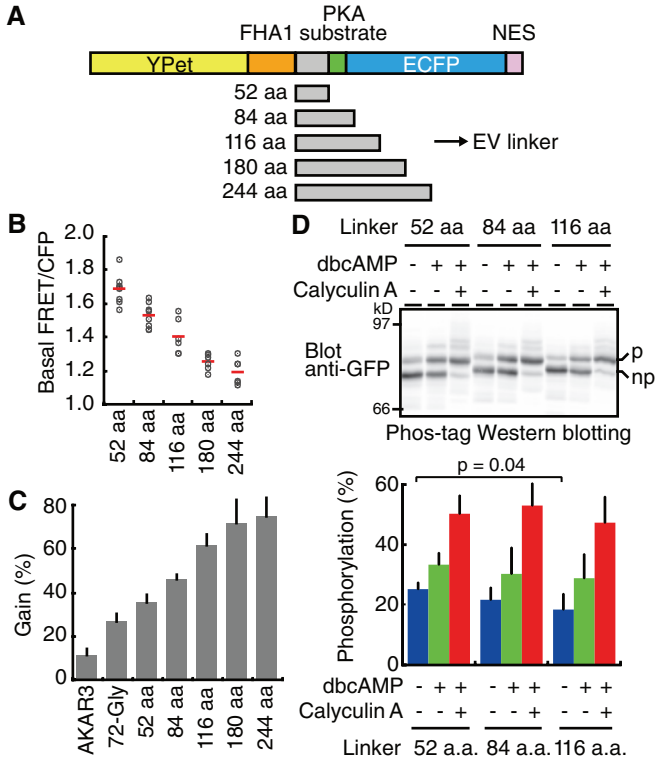

FIGURE 3: Effect of long linkers on the FRET gain. (A) Scheme of the PKA activity sensor consisting of YPet and ECFP. (B) HeLa cells expressing AKAR3 with a linker of various lengths were imaged by FRET microscopy to obtain the basal FRET/CFP. Each dot corresponds to the value from a single cell (n > 5). Horizontal bars are the mean values. (C) HeLa cells expressing a PKA sensor as indicated were stimulated with 1 mM dbcAMP for 10 min. The gain in FRET/CFP is represented with the SD (n > 5). (D) HeLa cells expressing AKAR3 with 52, 84, or 116 a.a. length of linker were stimulated with 1 mM dbcAMP or 1 mM dbcAMP and 50 nM Calyculin A for 10 min. Top, cell lysates were subjected to Phos-tag immunoblotting analysis with an anti-GFP antibody and a fluorescence-tagged secondary antibody. Tositions of phosphorylated (p) and nonphosphorylated biosensors (np) are indicated on the right of the representative gel image. Bottom, average values of the fraction of phosphorylated biosensors are shown with SD for three independent experiments. P value was calculated by a one-tailed paired *t* test.

cells stimulated with dibutyryl-cyclical AMP (dbcAMP), a membrane-permeable cAMP analogue. Except for the biosensor containing cp50Venus as the acceptor, the FRET/CFP ratio was increased upon dbcAMP stimulation in all biosensors. Among them, the FRET biosensors containing ECFP/YPet and Turquoise-GL/YPet exhibited the largest gain in FRET/CFP (Figure 2B). A substantial amount of the FRET biosensor with CyPet/YPet was cleaved at the linker region via a currently unknown mechanism (Supplemental Figure S1). Notably, YPet did not show any superiority to Venus when mTFP, an FP derived from coral (Ai *et al.*, 2006), was used as the donor (Figure 2, A and C), suggesting that a pair of dimerization-prone FPs is suitable for a distance-dependent FRET biosensor (see *Discussion*). Taken together, these results led us to conclude that the ECFP/YPet or Turquoise-GL/YPet pair was suitable for the donor and acceptor pair of the distance-dependent intramolecular FRET biosensor.

Optimization of the length of flexible linkers

Previously we showed that the basal GTP/GDP ratio of the Ras FRET biosensor was markedly larger than that of the endogenous Ras protein, implicating that the close proximity of the sensor and ligand domains could increase the proportion of FRET biosensors in the ON state (Mochizuki *et al.*, 2001), probably because the ligand domain competitively inhibits access of GTPase-activating proteins (GAPs) to the biosensor. This observation prompted us to lengthen the linker to reduce the proportion of ON state FRET biosensors (Figure 3A). In a preliminary experiment, linkers consisting of $(SAGG)_n$, where n indicates the number of repeats, served better than the 72 a.a. polyglycine linkers (Levskaya *et al.*, 2009; data not shown). Thus we prepared $(SAGG)_n$ linkers (n = 13–61) and inserted them into the prototype PKA biosensor. As expected, FRET/CFP in the absence of stimulation correlated inversely with the length of the linker (Figure 3B and Supplemental Figure S2). The gain of the FRET biosensors upon dbcAMP stimulation correlated with the length of the linker owing to the decrease in FRET/CFP in the absence of dbcAMP (Figure 3C).

The observed decrease of FRET/CFP before stimulation could be caused by two mechanisms. First, the long linker might reduce FRET efficiency simply by increasing the distance between CFP and YFP in the OFF state. Second, the long linker might reduce the fraction of ON state FRET biosensors in the basal state. To clarify which mechanism pertained, we separated the phosphorylated FRET biosensor from the nonphosphorylated one in HeLa cell lysates with SDS polyacrylamide gels containing a phosphorylated amino acid chelator, Phos-tag (Kinoshita *et al.*, 2006; Figure 3D). The 116 a.a. linker markedly reduced the basal phosphorylation level in

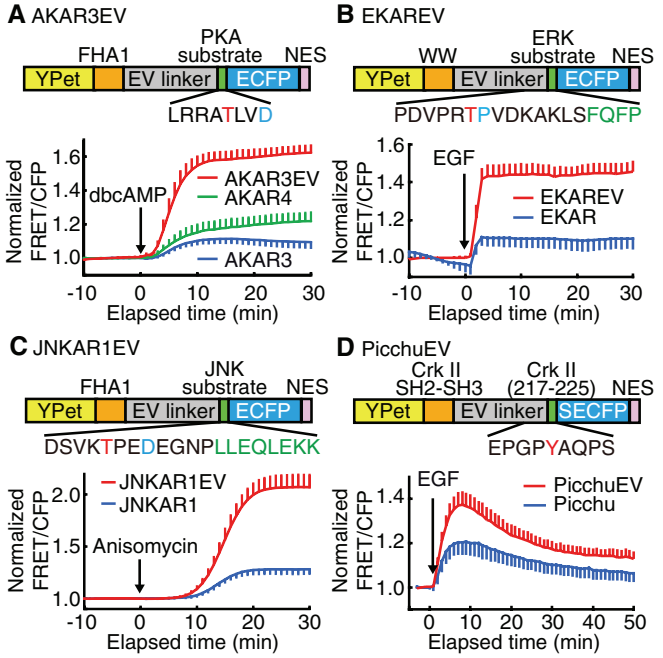

FIGURE 4: Improvement of FRET biosensors by the Eevee backbone. At the top of each panel, the structure of novel biosensors based on the Eevee backbone is shown. In the substrate peptide sequences, red letters indicate the phosphorylation site. Blue letters indicate amino-acid substitutions to increase the affinity to either the FHA1 or WW domain. Green letters indicate the docking site of the kinases. (A) HeLa cells expressing AKAR3EV, AKAR3, or AKAR4 were stimulated with 1 mM dbcAMP and time lapse–imaged by FRET microscopy (Supplemental Video S1). The FRET/CFP ratio of each cell was normalized by dividing by the averaged FRET/CFP value before stimulation. The mean and SD from at least 10 cells are plotted against time. (B) HeLa cells expressing EKAREV or EKAR were stimulated with 10 ng/ml EGF (Supplemental Video S2). The average of normalized FRET/CFP ratio is shown with SD ($n > 10$). (C) HeLa cells expressing JNKAR1EV or JNKAR1 were stimulated with 1 μg/ml Anisomycin (Supplemental Video S3). The average of normalized FRET/CFP ratio is shown with SD ($n > 10$). (D) HeLa cells expressing PicchuEV, an EGFR/Abl kinase sensor, or Picchu were stimulated with 25 ng/ml EGF (Supplemental Video S4). The average of normalized FRET/CFP ratio is shown with SD ($n > 10$).

comparison with the 52 a.a. linker. Because the reduction of the phosphorylated biosensor in the presence of dbcAMP was much lower, the gain of the biosensor containing the 116 a.a. linker was larger than that of the biosensors containing shorter linkers (Figure 3D). The levels of phosphorylated biosensors in the presence of the Ser/Thr phosphatase inhibitor, Calyculin A, were almost equal among the three biosensors. These results indicated that the preferable effect of the long linker was brought about by reducing the fraction of ON state FRET biosensors in the basal state (Figure 3D).

Through these analyses, we established the optimized backbone of the distance-dependent intramolecular FRET biosensors, consisting of a long, flexible linker and an optimized pair of FPs. This system was designated as the extension for enhanced visualization by evading extraFRET (Eevee). We also named the long linkers "EV linkers." Because the increase in the gain reached a zenith at 116 a.a. (Figure 3C), we used this linker in the following study.

Mathematical validation of the Eevee backbone system

To understand the mode of action of the Eevee backbone, we built and simulated a mathematical model of distance-dependent intramolecular FRET biosensors (see Supplemental Information). Computer simulations suggested that linker length and FP dimerization exerted distinct effects of FRET increase: sensitivity and dynamic range (Supplemental Figure S3, A–C). More importantly, these numerical simulations predicted the presence of an optimal length of linker to obtain the maximal gain of FRET, depending on the strength of FP dimerization (Supplemental Figure S3D). In line with this prediction, the dimerization-prone FP pair (i.e., YPet/ECFP) demonstrated a higher gain for longer length of linker in comparison to the Venus/ECFP pair (Supplemental Figure S3E). Convincingly, a gain of AKAR3 with Venus/ECFP was saturated at the linker length of 84 a.a., showing that the gain of the biosensor reached its highest point (Supplemental Figure S3E). Thus this simple simulation provided a plausible model to understand the mechanism by which the combination of EV linker and the dimerization-prone FPs increased the gain of distance-dependent intramolecular FRET biosensor.

FRET biosensors of kinases containing the Eevee backbone

To demonstrate proof of concept of the Eevee backbone, we applied the backbone to the previously reported FRET biosensors of protein kinases, an ERK sensor EKAR (Harvey *et al.*, 2008) and a JNK sensor JNKAR1 (Fosbrink *et al.*, 2010). The new FRET biosensors of PKA, ERK, and JNK were named AKAR3EV, EKAREV, and JNKAR1EV, respectively. HeLa cells expressing FRET biosensors were time lapse–imaged and stimulated (Figure 4). The gain of AKAR3EV was approximately sixfold and threefold larger than that of the original AKAR3 and AKAR4, respectively (Allen and Zhang, 2006; Depry *et al.*, 2011; Figure 4A and Supplemental Video S1). Similarly, the gains of EKAREV and JNKAR1EV were larger than those of EKAR and JNKAR1 by four- and threefold, respectively (Figure 4, B and C, and Supplemental Videos S2 and S3). We also found that, in EKAREV, either the FHA1 or WW domain was equally used as the phosphopeptide binding (ligand) domain (data not shown).

The Eevee backbone was also applied to Picchu, an EGFR and Abl tyrosine kinase activity sensor (Kurokawa *et al.*, 2001). In Picchu with an EV linker, the SH2–SH3 region and the substrate peptide (a.a. residues 217–225) of human CrkII were used as the ligand domain and sensor domain, respectively. The resulting PicchuEV exhibited a twofold increase in the gain in EGF-stimulated HeLa cells in comparison to the original Picchu (Figure 4D and Supplemental Video S4). Notably, the time course of FRET/CFP was similar between Picchu and PicchuEV (Figure 4D), suggesting that PicchuEV was also capable of monitoring the rapid kinetics of regulation in the protein kinases and phosphatases like the prototype Picchu.

FRET biosensors of small GTPases based on the Eevee backbone

We further applied the Eevee backbone to the intramolecular FRET biosensors of small GTPases. As examples, we adduced the FRET biosensors for Ras and Rac1, Raichu-Ras and Raichu-Rac1, respectively (Mochizuki *et al.*, 2001; Itoh *et al.*, 2002). The new FRET biosensors, RaichuEV-Ras and RaichuEV-Rac1, exhibited two- to threefold larger gains than the original FRET biosensors (Figure 5 and Supplemental Videos S5 and S6). Similarly to AKAR3 with the long linker (Figure 3C), the basal FRET/CFP ratio of Raichu-Ras with the EV linker was considerably reduced by the EV linker (Figure 5C). As expected, the basal FRET/CFP of RaichuEV-Rac1 was also markedly lower than that of the original Raichu-Rac1 (Figure 5F). We further confirmed that the EV linker reduced the ratio of GTP versus GDP bound to biosensors by thin-layer chromatography with the $^{32}P_i$-labeled, unstimulated HeLa cells (Supplemental Figure S4). Thus, in

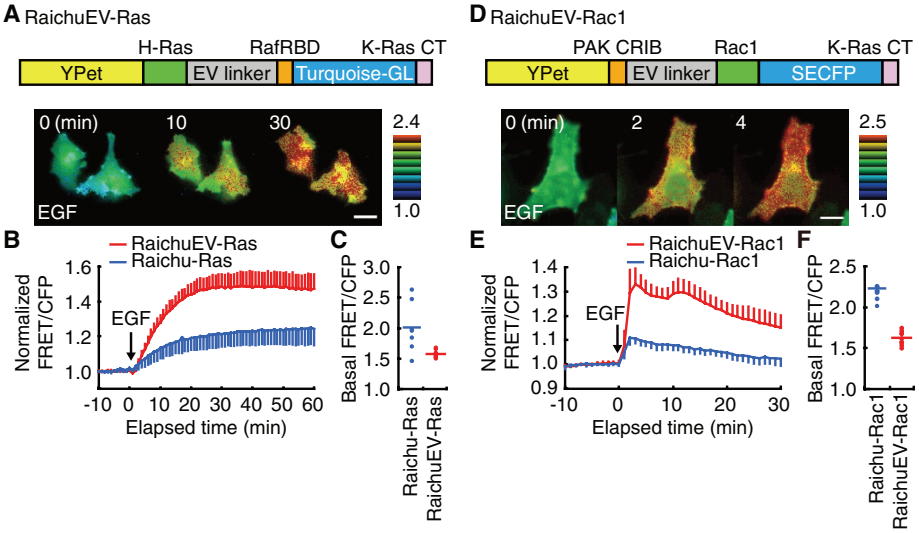

FIGURE 5: FRET biosensors of small GTPases based on the Eevee backbone. Structures of FRET biosensors based on the Eevee backbone, RaichuEV, are shown at the top of panels (A) and (D). RafRBD and PAK CRIB denote the Ras-binding domain of Raf1 and the Cdc42/Rac-interactive binding domain, respectively. Cos7 cells expressing RaichuEV or the prototype Raichu were stimulated with 50 ng/ml EGF and time lapse–imaged (Supplemental Videos S5 and S6). Representative FRET/CFP ratio images are shown in the intensity-modulated display mode. Scale bars are 10 μm. (B and E) The FRET/CFP ratio of each cell was normalized by dividing by the averaged FRET/CFP value before stimulation. The mean and SD from at least 10 cells are plotted against time. (C and F) Basal FRET/CFP ratios of RaichuEV and Raichu are plotted. Each dot corresponds to the value from a single cell, and at least six cells were analyzed. The horizontal bar indicates the mean.

analogy to AKAR3EV, the EV linker seemed to facilitate the access of GAP, leading to a reduction in the GTP-bound ON state of Raichu under the basal condition.

Rapid development of new FRET biosensors by the Eevee backbone

We tried to develop novel Ser/Thr kinase activity sensors for RSK, S6K, Akt, and classical PKC by using the Eevee backbone (Figure 6). Because the orientation-dependent FRET could be neglected in the Eevee backbone, we simply needed to determine the optimal substrate peptide specific to each kinase and the appropriate phosphate-binding domain for that peptide sequence. For example, we chose substrate peptides encompassing Ser-1798 of TSC2 (Roux *et al.*, 2004) and Thr-1135 of Rictor (Dibble *et al.*, 2009) for the development of Eevee-RSK and -S6K, respectively. HeLa cells expressing these FRET biosensors were stimulated with EGF and, after 10 or 30 min, inhibited with either BI-D1780 or rapamycin (Figure 6, A–F, and Supplemental Videos S7 and S8). We observed the apparent increase in FRET/CFP upon EGF stimulation with Eevee-RSK and -S6K. The effect of the inhibitors was also clearly demonstrated. This result indicated that the Eevee backbone provided an easy and rapid method for the development of FRET biosensors.

Such simple application of the Eevee backbone might not always guarantee a large gain, however, as we show in the case of FRET biosensors of Akt and PKCβ developed by the same approach. The substrate peptides were from previously reported consensus sequences of Akt (Obata *et al.*, 2000) and MARCKS, respectively (Violin *et al.*, 2003; Kunkel *et al.*, 2005). The gains of Akt and PKC FRET sensors, Eevee-Akt-cyt and Eevee-PKC-cyt, were 8 and 4% in EGF-stimulated Cos7 cells and tetradecanoylphorbol 13-acetate (TPA)-stimulated HeLa cells, respectively (Supplemental Figure S5). These gains were markedly lower than those of the other Eevee biosensors. To increase the fraction of the phosphorylated FRET biosensor, we added the Pleckstrin homology (PH) domain of Akt to the N terminus of the FRET biosensors of Akt (Figure 6G). The PH domain binds to phosphatidylinositol (3,4,5)-trisphosphates and serves as a plasma membrane–targeting signal. Hence, addition of the PH domain to the FRET biosensors of Akt could increase the effective concentration of the FRET biosensor around the active Akt at the plasma membrane. As expected, cells expressing this FRET biosensor, which we named Eevee-Akt, exhibited a rapid and robust increase in FRET/CFP (ca. 25%) at the plasma membrane (Figure 6, H and I, and Supplemental Video S9). As a control, we prepared Eevee-Akt-TA, in which Thr in the substrate peptide was replaced with Ala. Unexpectedly, we found that Eevee-Akt-TA also exhibited an 18% increase in FRET/CFP ratio upon stimulation (Figure 6H). This increase in FRET/CFP was probably caused by the bystander FRET (i.e., local increase in the concentration of the FRET biosensors at the plasma membrane could result in the stochastic intermolecular FRET; Supplemental Figure S6; Chiu *et al.*, 2002).

In a similar manner, we constructed Eevee-PKCβ, in which the C1 domain of PKCβ was fused at the N terminus of the FRET biosensor (Figure 6J). The C1 domain binds to diacylglycerol and serves as another plasma membrane–targeting signal. Again, cells expressing Eevee-PKC exhibited a rapid and marked increase in FRET/CFP (Figure 6L and Supplemental Video S10). Similarly to Eevee-Akt-TA, Eevee-PKC-TA also showed membrane translocation (Supplemental Figure S6) and a slight, but not ignorable, increase in FRET/CFP ratio (Figure 6K). Taken together, Eevee-PKC and Eevee-Akt monitor not only kinase activity of PKC and Akt, but also stimulation-dependent membrane translocation of the kinases. Furthermore, we constructed the Akt and PKC biosensors that were localized to plasma membrane by lipid modification of the K-Ras4B C-terminus region (Eevee-Akt-pm and Eevee-PKC-pm; Supplemental Figure 5). TA mutants of these plasma membrane–targeted FRET biosensors did not respond to the stimulation. Notably, FRET gains of Eevee-Akt-pm and Eevee-PKC-pm upon stimulation corresponded to the difference of FRET gains between Eevee-Akt and Eevee-Akt-TA and between Eevee-PKC and Eevee-PKC-TA (Supplemental Figure S7). Thus Eevee-PKC-pm and Eevee-Akt-pm are applicable to visualize only the kinase activity of PKC and Akt at the plasma membrane, respectively.

Quantitative evaluation of kinase inhibitors by Eevee biosensor-expressing cell lines

With FRET biosensors having large gains in hand, we developed a quantitative and rapid assay to evaluate the effects of kinase inhibitor on Ser/Thr kinases in living cells. First, we established HeLa cell lines stably expressing Eevee biosensors. We previously failed to establish such stable cell lines with retrovirus/lentivirus-mediated gene transfer or by the transfection of linearized plasmid DNAs because of frequent recombination between YFP and CFP (data not shown). We recently found that this problem could be readily overcome by the use of a *piggyBac* transposase system (Yusa *et al.*,

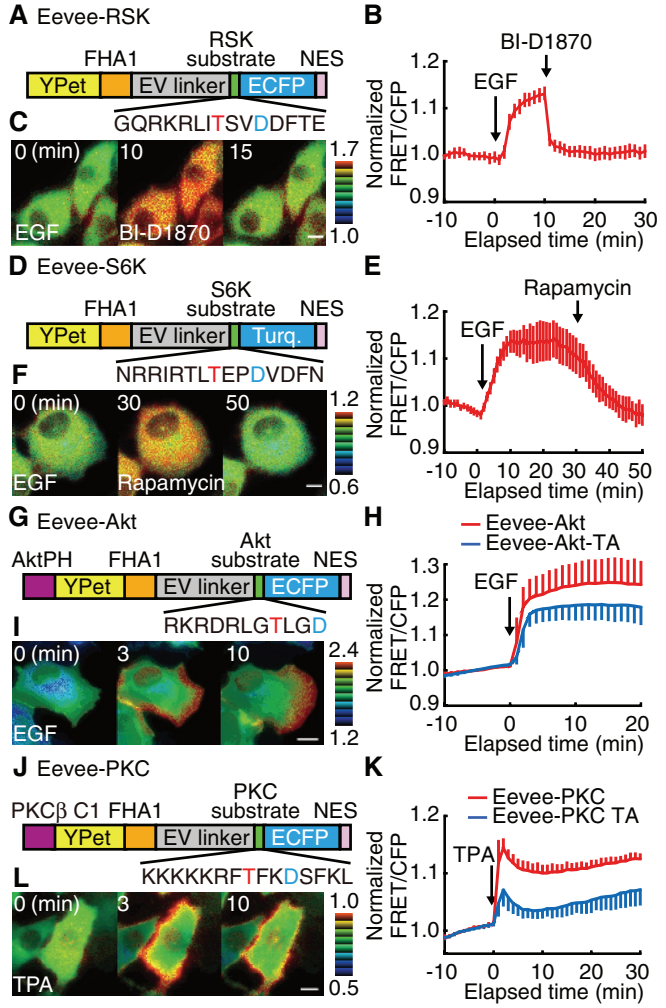

FIGURE 6: Novel Ser/Thr kinase FRET biosensors based on the Eevee backbone. (A, D, G, and J) Structures of Eevee-RSK, Eevee-S6K, Eevee-Akt, and Eevee-PKC, which are FRET biosensors of RSK, S6K, Akt, and classical PKC activities, respectively. Red and blue letters in the substrate peptide sequences denote the phosphorylation sites and amino-acid substitutions to increase the affinity to FHA1. (B, E, H, and K) HeLa cells expressing Eevee-RSK (B), Eevee-S6K (E), Eevee-PKC (K), or Cos7 cells expressing Eevee-Akt (H) were time lapse–imaged and stimulated with 10 ng/ml EGF (B and E), 50 ng/ml EGF (H), or 1 μM TPA (K). Cells expressing Eevee-RSK and Eevee-S6K were further treated with 10 nM BI-D1870 (B) and 100 nM rapamycin (E), respectively, at 30 min after EGF stimulation. The FRET/CFP ratio of each cell was normalized by dividing by the averaged FRET/CFP value before stimulation (Supplemental Videos S7–S10). The mean and SD from at least 10 cells are plotted against time. (C, F, I, and L) Representative FRET/CFP ratio images with Eevee-RSK (C), Eevee-S6K (F), Eevee-Akt (I), and Eevee-PKC (L) are shown in the intensity-modulated display mode. Scale bars are 10 μm.

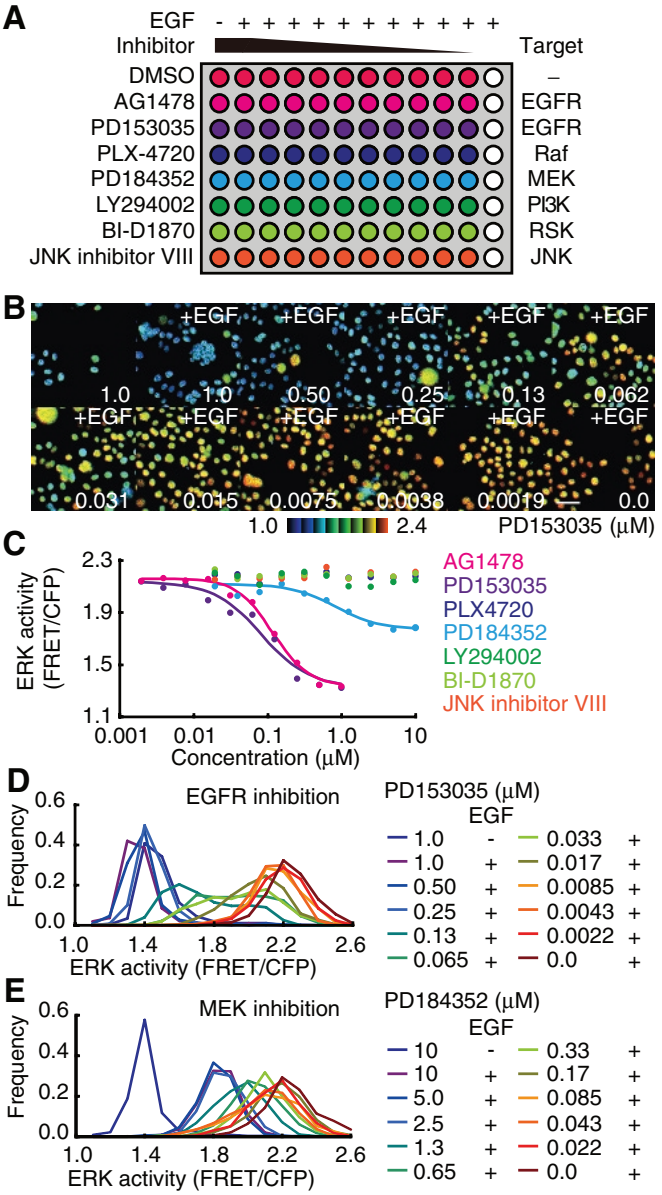

FIGURE 7: Quantitative evaluation of kinase inhibitors with Eevee-expressing cell lines. (A) Schematic view of the experimental design. Cells expressing EKAREV-nuc were seeded, starved, and treated with stimulant in the presence of decreasing concentrations of the indicated kinase inhibitors. After 30 min, FRET images were acquired and processed for quantification. (B) Shown here are the representative FRET/CFP ratio images of HeLa cells stably expressing EKAREV-nuc and treated with 25 ng/ml EGF and the indicated concentrations of an EGFR inhibitor, PD153035. Scale bar is 50 μm. (C) Averaged FRET/CFP ratios are plotted against the concentrations of kinase inhibitors and fitted with curves by the four-parameter logistic model. (D and E) FRET/CFP ratios in each cell at the indicated concentration of PD153035 (D) or a MEK inhibitor, PD184352 (E), were quantified and represented in histograms (n > 80 cells).

2009). After single-cell cloning, the cells were seeded onto a 96-well glass base plate and treated with stimulants and kinase inhibitors (Figure 7A). For example, cells expressing EKAREV-nuc, which localized to nucleus, were stimulated with EGF in the presence of decreasing concentrations of various inhibitors and FRET-imaged by an automated epifluorescence microscope (Figure 7B and Supplemental Figure S8). By computer-assisted processing of the FRET/CFP ratio of each cell, we could obtain the IC50 values of kinase inhibitors (Figure 7C). Intriguingly, this single cell–based assay also revealed unexpected differences in terms of the mode of action of the inhibitors. EGF receptor inhibitors such as AG1478 and PD153035 inhibited ERK activity as a bistable (all-or-nothing) response, whereas the MEK inhibitor PD184352 inhibited ERK with a graded response (Figure 7, D and E, and Supplemental Figure S9). Taken together, these results demonstrated that the Eevee system combined with *piggyBac* transposase enabled rapid and quantitative evaluation of the effect of drugs in living cells.

DISCUSSION

We have developed an optimized backbone, Eevee, which allows us to quickly develop FRET biosensors. The flexible long linker and the optimized FP pairs cooperatively served to increase the gain of the FRET biosensors. The Eevee backbone was used to improve FRET biosensors of PKA, ERK, JNK, EGFR/Abl, Ras, and Rac1 (Figures 4 and 5) and to develop FRET biosensors of RSK, S6K, Akt, and PKC (Figure 6).

The key technology of the Eevee backbone is the flexible long linker EV, which renders FRET biosensors mostly distance-dependent. It has been reported that circularly permutated (cp) FPs improved FRET biosensors of calcium and PKA (Nagai *et al.*, 2004; Allen and Zhang, 2006), which would seem to provide evidence that orientation has a critical impact on the FRET efficiency of the intramolecular FRET biosensors. Consistent with this idea, the FRET efficiency of orientation-dependent biosensors has been reported to be drastically influenced by the addition or deletion of one to several amino acids at the C terminus of FPs (Miyawaki *et al.*, 1997; Horikawa *et al.*, 2010). The developer, however, could not predict whether the FRET of a newly constructed, orientation-dependent biosensor would increase or decrease upon the perception of the signal (Violin *et al.*, 2003; Kunkel *et al.*, 2005). For this reason, we decided to provide an optimized backbone for the distance-dependent type of FRET biosensor. The evidence that FRET of the Eevee backbone is mostly distance-dependent is as follows: 1) All of the FRET biosensors based on the Eevee backbone were associated with an increase in FRET/CFP in the ON state; 2) the basal fraction of OFF-state biosensors was inversely correlated with the length of the linker (Figure 3C); and 3) a series of cpVenus variants did not improve the gain (Figure 2B). Of note, there existed optimal linker lengths, depending on the pair of FPs, which were qualitatively explained by the mathematical model (Supplemental Figure S3). To quantitatively predict an optimal length of linker, we need to measure and/or estimate quantitative parameters and implement a model with those parameters.

An intramolecular FRET biosensor often suffers from a high basal FRET level, which could be caused by two mechanisms. First, the distance between the donor and acceptor FPs may not be sufficient to eliminate the basal FRET. Second, and more likely, the ligand domain may increase the fraction of ON-state biosensors by masking the sensor domain from negative regulators such as phosphatases and GAPs. Consistent with this idea, the basal GTP/GDP ratio on the Raichu-RhoA biosensor varies significantly according to the affinity of RhoA binding domains for RhoA (Yoshizaki *et al.*, 2003). We presume that a flexible long linker minimizes this masking effect by reducing the effective concentration of the ligand domain around the sensor domain. There have been several reports of a linker peptide improving the FRET biosensor. For example, a "flip-flop" linker composed of a rigid α-helical linker with a flexible diglycine motif (Sato *et al.*, 2003) and an "elastic" linker derived from spider silk protein flagelliform (Grashoff *et al.*, 2010) have been shown to increase the gain of the FRET biosensor. It is unknown, however, whether these linkers also serve to reduce the masking effect of the ligand domain.

We showed that two FP pairs, ECFP/YPet and Turquoise-GL/YPet, were used preferably to the distance-dependent intramolecular FRET biosensors (Ouyang *et al.*, 2008). The wild-type *Aequorea* FP forms a dimer with congeneric *Aequorea* FP at high concentration, of which the dissociation constant (K_d) is 110 μM (Zacharias *et al.*, 2002). Recently Kotera *et al.* (2010) have verified that an *Aequorea* FP pair possessing reversible dimerization property enhances FRET of intramolecular FRET biosensors. Originally, YPet was reported to enhance FRET without inducing heterodimerization between YPet and CyPet in an intermolecular FRET biosensor (Nguyen and Daugherty, 2005). Recent reports suggested, however, that the increase in FRET gain by using YPet as an acceptor seems to be attributable to an enhanced dimerization with the congeneric FPs (Ohashi *et al.*, 2007; Kotera *et al.*, 2010). In agreement with this report, we have found that YPet did not improve FRET when a TFP, which was derived from *Clavularia* FP (Ai *et al.*, 2006), was used as a donor (Figure 2C). It should be noted that, beyond a certain threshold, the increasing donor–acceptor FP binding affinity will yield a substantial fraction of FRET biosensors locked to the closed form even in the absence of stimulation.

To develop a novel FRET biosensor of Ser/Thr kinase with the Eevee backbone, we need to find a substrate peptide that is phosphorylated by the said Ser/Thr kinase with high efficiency and specificity. We will adduce S6K as an example. Because the two major substrates of S6K are S6 and Rictor (Ferrari *et al.*, 1991; Dibble *et al.*, 2009), naturally we chose a substrate peptide encompassing Ser-240 of S6 and Thr-1135 of Rictor. Interestingly, the FRET biosensor containing the substrate peptide derived from Rictor exhibited a significant response to EGF and rapamycin (Figure 6), whereas the other FRET biosensor containing a substrate peptide derived from S6 did not respond to EGF due to inefficient phosphorylation (data not shown). Notably, newly developed biosensors, Eevee-RSK, Eevee-S6K, Eevee-Akt, and Eevee-PKC, did not achieve gains as large as did AKAR3EV, EKAREV, and JNKAR1EV. This result is possibly due to the lower phosphorylation efficiency. Hence, screening of an optimal substrate peptide that is efficiently phosphorylated by the kinase of interest remains an important step in the development of FRET biosensors of a kinase. This problem of low phosphorylation efficiency may be overcome by two options. First, by the addition of a subcellular localization domain, the Eevee biosensor could be concentrated at the specific intracellular compartment where the said kinase is activated. Successful examples are Eevee-Akt and Eevee-PKC (Figure 6). Second, we may use a motif that facilitates the association of the substrate with the target kinase as exemplified in EKAREV and JNKAR1EV (Figure 4; Harvey *et al.*, 2008; Fosbrink *et al.*, 2010).

In summary, we described an optimized backbone for intramolecular FRET biosensors. The Eevee biosensor still needs a number of steps and careful characterization to create a sensitive and specific FRET biosensor, such as a choice of efficiently phosphorylated peptide and intracellular targeting. This simple and versatile system should prove useful for developing FRET biosensors with high productivity and for accelerating our understanding of spatiotemporal cellular signaling.

MATERIALS AND METHODS

FRET biosensor construction

The cDNAs of YFPs and CFPs were amplified by PCR. Fluorescence proteins used as acceptor or donor were Venus (Nagai *et al.*, 2002), cpVenus (cp50Venus, cp157Venus, cp173Venus, cp195Venus, cp229Venus; Nagai *et al.*, 2004), mCitrine (Griesbeck *et al.*, 2001), YPet, CyPet (Nguyen and Daugherty, 2005), mTFP1 (Ai *et al.*, 2006), mTurquoise, mTurquoise-GL (Goedhart *et al.*, 2010), ECFP, and SECFP (a brighter version of ECFP developed by A. Miyawaki [RIKEN, Saitama, Japan]). The cDNA of SECFP contains additional mutations of K26R, D130G, N165H, and S176G based on the cDNA of ECFP. mTurquoise and mTurquoise-GL were the gifts of T. W. J. Gadella, Jr. (Swammerdam Institute for Life Sciences, Amsterdam,

The Netherlands; Goedhart *et al.*, 2010). The mutation of Ala at the 206 position in mTurquoise and mTurquoise-GL was restored to Lys with a two-step overlap PCR, generating Turquoise and Turquoise-GL (Goedhart *et al.*, 2010). Amino acid substitutions in YFP and CFP variants used in this study are summarized in Supplemental Table S1. These cDNAs of fluorophores were inserted into the eukaryotic expression vectors pCAGGS (Niwa *et al.*, 1991) and/or pPBbsr, which harbors blasticidin S–resistant gene (Yusa *et al.*, 2009). The unique restriction enzyme sites are shown in Figure 1B. EKAR was obtained from Addgene (Cambridge, MA; http://www.addgene.org/). AKAR3, AKAR4, and JNKAR1 were gifts from J. Zhang (Johns Hopkins University, Baltimore, MD).

The flexible linkers collectively designated EV consisted of various numbers of the 20 a.a. peptide, SAGGSAGGSAGGSAGGSAGG (Levskaya *et al.*, 2009). The cDNAs of the EV were introduced into an expression plasmid by a combination of standard subcloning and annealed DNA duplex ligation. The DNA of the 20 a.a. EV linker was generated by annealing the sense-oligonucleotide (5′-GTACCAGTGCTGGTGGTAGTGCTGGTGGTAGTGCTGGTGGTAGTGCTGGTGGTT-3′) and antisense-oligonucleotide (5′-CCGGAACCACCAGCACTACCACCAGCACTACCACCAGCACTACCACCAGCACTACCACCAGCACTG-3′) and inserted into an expression vector of the PKA FRET biosensor, generating pAKAR3EV-20. pEevee-20 was cleaved with *Eco*RI/Aor13HI or *Eco*RI/Asp718I. Fragments containing the EV linker coding sequence were ligated with the following DNA, which was obtained by annealing (5′-CCGGCAGTGCTGGTGGTAGTGCTGGTGGTA-3′) and (5′-GTACTACCACCAGCACTACCACCAGCACTG-3′). The resulting plasmid was named pAKAR3EV-52, which contained a 52 a.a. linker. By repeating this step, we obtained expression plasmids containing EV linkers up to 244 a.a. in length.

The Ser/Thr kinase FRET biosensors with long linkers were collectively designated Eevee, and the plasmids thereof, pEevee, were constructed essentially in the manner of pRaichu-Ras (Mochizuki *et al.*, 2001). From the N terminus, Eevee consists of YPet (a.a. 1–238), a spacer (Leu-Glu), the FHA1 domain of yeast Rad53 (a.a. 241–382) used as the ligand domain, a spacer (Gly-Thr), an EV linker, a spacer (Ser-Gly), a Ser/Thr kinase substrate peptide used as the sensor domain, a spacer (Gly-Gly-Arg), ECFP (a.a. 513–750), a spacer (Ser-Arg), and the nuclear export sequence of the HIV–1 rev protein (LQLPPLERLTLD) or the nuclear localization signal of the SV40 large T antigen (GGPPKKKPKVEDP). Eevee–Akt and Eevee-PKC included the PH domain of human Akt1 (a.a. 5–152) and the C1 domain of human PKCβ (a.a. 5–121) at the N terminus of YPet, respectively. In EKAREV, the FHA1 domain was replaced with the WW domain of human Pin1 (a.a. 241–295). cDNAs of the substrate peptides were synthesized so that the amino acid residue at the phosphoacceptor was Thr and the amino acid at the +3 position from said Thr was Asp, rendering the substrate sequence optimal for the binding to the FHA1 domain. Similarly, the amino acid residue at the +1 position from the phosphoacceptor amino acid was substituted for Pro when the WW domain was used as the ligand domain. The synthesized oligonucleotides were annealed and inserted into the expression vector. The substrate peptide sequences used in this study are listed in Supplemental Table S2.

A plasmid encoding PicchuEV was generated as follows. The DNA fragment of human CrkII encompassing the SH2 domain and the SH3 domain (a.a. 1–204) was used as the ligand domain. The substrate peptide of human CrkII (a.a. 217–225) was used as the sensor domain. pRaichu-Ras and Raichu-Rac1 containing an EV linker were constructed by replacing the linker region of the original biosensors with an EV linker (Mochizuki *et al.*, 2001; Itoh *et al.*, 2002).

Cells, reagents, and antibodies

HeLa cells were purchased from the Human Science Research Resources Bank (Sennanshi, Japan). The Cos7 cells used were Cos7/E3, a subclone of Cos7 cells established by Y. Fukui (National Research Institute of Health, Taiwan, Republic of China). HeLa cells and Cos7 cells were maintained in DMEM (Sigma-Aldrich, St. Louis, MO) supplemented with 10% FBS. The cells were plated on 35-mm glass base dishes or 96-well glass base plates (Asahi Techno Glass, Tokyo, Japan), which were coated with collagen type I (Nitta Gelatin, Osaka, Japan). Plasmids encoding FRET biosensors were transfected into HeLa cells and Cos7 cells by 293fectin or Lipofectamine 2000, according to the manufacturer's instructions (Invitrogen, San Diego, CA), respectively. EGF was purchased from Sigma-Aldrich. dbcAMP, TPA, Calyculin A, Anisomycin, PD153035, and JNK inhibitor VIII were purchased from Calbiochem (La Jolla, CA). PD184352 was obtained from Toronto Research Chemicals (Ontario, Canada). BI-D1870 was purchased from Symansis (Shanghai, China). Rapamycin was obtained from LC Laboratories (Woburn, MA). PLX-4720 was purchased from Selleck Chemicals (Houston, TX). The expression vector of *piggyBac* transposase was provided by A. Bradley (Wellcome Trust Sanger Institute, Cambridge, UK; Yusa *et al.*, 2009). Phos-tag was obtained from the Phos-tag Consortium (Hiroshima, Japan; www.phos-tag.com). Anti-green fluorescence protein (GFP) sera were prepared in our laboratory. LI-COR (Lincoln, NE) blocking buffer and the IRDye680- and IRDye800-conjugated anti–rabbit and anti–mouse immunoglobulin G secondary antibodies were obtained from LI-COR.

Phospho-affinity PAGE

Phospho-affinity gel electrophoresis was performed essentially as described previously (Kinoshita *et al.*, 2006). Conventional SDS-polyacrylamide separation gels were supplemented with 50 μM Phos-tag and 100 μM $MnCl_2$, according to the manufacturer's protocol. Proteins were detected and quantified by using an Odyssey Infrared Imaging System (LI-COR).

Time-lapse FRET imaging

FRET images were obtained and processed using essentially the same conditions and procedures as previously reported (Aoki and Matsuda, 2009). Briefly, HeLa cells or Cos7 cells expressing FRET biosensors were starved for 6–12 h with phenol red–free DMEM/F12 medium or Medium 199 (Invitrogen) containing 0.1% bovine serum albumin (BSA) or phenol red–free M199 (Invitrogen) with 20 mM HEPES and 0.1% BSA. Starved cells were treated with stimulus, followed by the addition of inhibitors if necessary. Cells were imaged with an inverted microscope (IX71 or IX81; Olympus, Tokyo, Japan) equipped with a 60× objective lens (Olympus), a cooled CCD camera (CoolSNAP HQ or CoolSNAP K4; Roper Scientific, Tucson, AZ), an LED illumination system (CoolLED precisExcite; Molecular Devices, Sunnyvale, CA), an IX2-ZDC laser-based autofocusing system (Olympus), and an MD-XY30100T-Meta automatically programmable XY stage (SIGMA KOKI, Tokyo, Japan). The following filters used for the dual-emission imaging studies were obtained from Omega Optical (Brattleboro, VT): an XF1071 (440AF21) excitation filter, an XF2034 (455DRLP) dichroic mirror, and two emission filters (XF3075 480AF30 for CFP and XF3079 535AF26 for YFP). After background subtraction, FRET/CFP ratio images were created with MetaMorph software (Universal Imaging, West Chester, PA), and represented by the intensity-modulated display mode. In the

intensity-modulated display mode, eight colors from red to blue are used to represent the FRET/CFP ratio, with the intensity of each color indicating the mean intensity of FRET and CFP. For the quantification, the FRET and CFP intensities were averaged over the whole cell area, and the results were exported to Excel software (Microsoft Corporation, Redmond, WA). In some experiments, the FRET/CFP value from before 10 min to the time of stimulation was averaged and used as the reference. The ratio of raw FRET/CFP value versus the reference value was defined as the normalized FRET/CFP value.

Multiwell FRET imaging

A HeLa cell line stably expressing EKAREV-nls, which contained the nuclear localization signal, was established according to Yusa *et al*. (2009). The cells were seeded on a 96-well glass base plate at a cell density of 1.5×10^4 cells/well. One day after seeding, the cells were serum starved for 6 h, followed by treatment with stimulant and kinase inhibitors for 15 min. Then, the 96-well plate was imaged by an inverted microscope as described earlier in text, except that an 20× objective lens was used. FRET and CFP images were obtained in one position for every well of the 96-well plate.

Spectroscopy by confocal microscopy

Twenty-four hours after transfection, HeLa cells expressing FRET probes were starved for 3–6 h. Fluorescence spectra were acquired by using a FV-1000 confocal imaging system (Olympus) in the lambda scanning mode upon excitation of CFP at a wavelength of 405 nm.

Quantification of guanine nucleotide bound to GTPases

Guanine nucleotides bound to Raichu biosensors were analyzed essentially as described previously (Gotoh *et al*., 1997). Briefly, HeLa cells were transfected with expression vectors for Raichu-Ras, RaichuEV-Ras, Raichu-Rac1, and RaichuEV-Rac1. After 36 h, the cells were metabolically labeled with $^{32}P_i$ orthophosphate for 2 h and then lysed. The cell lysates were clarified by centrifugation, and Raichu biosensors were immunoprecipitated by using anti-GFP antiserum. Guanine nucleotides bound to Raichu biosensors were separated by thin-layer chromatography and quantitated with a BAS-1000 image analyzer (Fujifilm, Tokyo, Japan).

Mathematical and statistical analysis

Simulation was implemented by Mathematica software (Wolfram Research, Champaign, IL). Details are described in the Supplemental Information.

Phosphorylation levels (Figure 3) or GTP/(GTP+GDP) levels (Supplemental Figure S4) at the basal state varied from day to day; the reason for this variation is not clear. Thus we could not combine all data obtained in 3–4 d and we had to handle the data obtained in one experiment as one data set. In this case, a paired *t* test needed to be applied to examine a statistical significance. The paired *t* test demonstrated whether a long linker decreased the basal phosphorylation and GTP/(GTP+GDP) levels. In addition, a long linker was involved in a decrease of basal FRET level, suggesting that the long linker decreased basal phosphorylation level (Figure 3) and basal GTP/(GTP+GDP) level (Supplemental Figure S4). Therefore a one-tailed *t* test was applied to the analysis.

ACKNOWLEDGMENTS

We thank A. Miyawaki, T. Akagi, J. Miyazaki, K. Yusa, A. Bradley, J. Zhang, K. Svoboda, and T. W. J. Gadella, Jr., for the plasmids. K. Morita, Y. Inaoka, K. Hirano, R. Sakai, N. Nonaka, and A. Kawagishi are also to be thanked for their technical assistance. We are grateful to the members of the Matsuda Laboratory for their helpful input. K.A. was supported by a Grant-in-Aid for Scientific Research on Priority Areas and by the JST PRESTO program. M.M. was supported by the Research Program of Innovative Cell Biology by Innovative Technology (Cell Innovation) from the Ministry of Education, Culture, Sports, and Science (MEXT), Japan.

REFERENCES

Ai HW, Henderson JN, Remington SJ, Campbell RE (2006). Directed evolution of a monomeric, bright and photostable version of Clavularia cyan fluorescent protein: structural characterization and applications in fluorescence imaging. Biochem J 400, 531–540.

Allen MD, Zhang J (2006). Subcellular dynamics of protein kinase A activity visualized by FRET-based reporters. Biochem Biophys Res Commun 348, 716–721.

Aoki K, Kiyokawa E, Nakamura T, Matsuda M (2008). Visualization of growth signal transduction cascades in living cells with genetically encoded probes based on Forster resonance energy transfer. Philos Trans R Soc Lond B Biol Sci 363, 2143–2151.

Aoki K, Matsuda M (2009). Visualization of small GTPase activity with fluorescence resonance energy transfer-based biosensors. Nat Protoc 4, 1623–1631.

Chiu VK, Bivona T, Hach A, Sajous JB, Silletti J, Wiener H, Johnson RL, 2nd, Cox AD, Philips MR (2002). Ras signalling on the endoplasmic reticulum and the Golgi. Nat Cell Biol 4, 343–350.

Depry C, Allen MD, Zhang J (2011). Visualization of PKA activity in plasma membrane microdomains. Mol Biosyst 7, 52–58.

Dibble CC, Asara JM, Manning BD (2009). Characterization of Rictor phosphorylation sites reveals direct regulation of mTOR complex 2 by S6K1. Mol Cell Biol 29, 5657–5670.

Ferrari S, Bandi HR, Hofsteenge J, Bussian BM, Thomas G (1991). Mitogen-activated 70K S6 kinaseIdentification of in vitro 40 S ribosomal S6 phosphorylation sites. J Biol Chem 266, 22770–22775.

Fosbrink M, Aye-Han NN, Cheong R, Levchenko A, Zhang J (2010). Visualization of JNK activity dynamics with a genetically encoded fluorescent biosensor. Proc Natl Acad Sci USA 107, 5459–5464.

Goedhart J, van Weeren L, Hink MA, Vischer NO, Jalink K, Gadella TW, Jr (2010). Bright cyan fluorescent protein variants identified by fluorescence lifetime screening. Nat Methods 7, 137–139.

Gotoh T, Niino Y, Tokuda M, Hatase O, Nakamura S, Matsuda M, Hattori S (1997). Activation of R-Ras by Ras-guanine nucleotide-releasing factor. J Biol Chem 272, 18602–18607.

Grashoff C *et al*. (2010). Measuring mechanical tension across vinculin reveals regulation of focal adhesion dynamics. Nature 466, 263–266.

Griesbeck O, Baird GS, Campbell RE, Zacharias DA, Tsien RY (2001). Reducing the environmental sensitivity of yellow fluorescent protein. Mechanism and applications. J Biol Chem 276, 29188–29194.

Harvey CD, Ehrhardt AG, Cellurale C, Zhong H, Yasuda R, Davis RJ, Svoboda K (2008). A genetically encoded fluorescent sensor of ERK activity. Proc Natl Acad Sci USA 105, 19264–19269.

Horikawa K, Yamada Y, Matsuda T, Kobayashi K, Hashimoto M, Matsu-Ura T, Miyawaki A, Michikawa T, Mikoshiba K, Nagai T (2010). Spontaneous network activity visualized by ultrasensitive Ca(2+) indicators, yellow Cameleon-Nano. Nat Methods 7, 729–732.

Itoh RE, Kurokawa K, Ohba Y, Yoshizaki H, Mochizuki N, Matsuda M (2002). Activation of rac and cdc42 video imaged by fluorescent resonance energy transfer-based single-molecule probes in the membrane of living cells. Mol Cell Biol 22, 6582–6591.

Jares-Erijman EA, Jovin TM (2003). FRET imaging. Nat Biotechnol 21, 1387–1395.

Karasawa S, Araki T, Nagai T, Mizuno H, Miyawaki A (2004). Cyan-emitting and orange-emitting fluorescent proteins as a donor/acceptor pair for fluorescence resonance energy transfer. Biochem J 381, 307–312.

Kinoshita E, Kinoshita-Kikuta E, Takiyama K, Koike T (2006). Phosphate-binding tag, a new tool to visualize phosphorylated proteins. Mol Cell Proteomics 5, 749–757.

Kotera I, Iwasaki T, Imamura H, Noji H, Nagai T (2010). Reversible dimerization of Aequorea victoria fluorescent proteins increases the dynamic range of FRET-based indicators. ACS Chem Biol 5, 215–222.

Kunkel MT, Ni Q, Tsien RY, Zhang J, Newton AC (2005). Spatio-temporal dynamics of protein kinase B/Akt signaling revealed by a genetically encoded fluorescent reporter. J Biol Chem 280, 5581–5587.

Kurokawa K, Mochizuki N, Ohba Y, Mizuno H, Miyawaki A, Matsuda M (2001). A pair of fluorescent resonance energy transfer-based probes

for tyrosine phosphorylation of the CrkII adaptor protein in vivo. J Biol Chem 276, 31305–31310.
Levskaya A, Weiner OD, Lim WA, Voigt CA (2009). Spatiotemporal control of cell signalling using a light-switchable protein interaction. Nature 461, 997–1001.
Li IT, Pham E, Truong K (2006). Protein biosensors based on the principle of fluorescence resonance energy transfer for monitoring cellular dynamics. Biotechnol Lett 28, 1971–1982.
Miyawaki A (2003). Visualization of the spatial and temporal dynamics of intracellular signaling. Dev Cell 4, 295–305.
Miyawaki A, Llopis J, Heim R, McCaffery JM, Adams JA, Ikura M, Tsien RY (1997). Fluorescent indicators for Ca2+ based on green fluorescent proteins and calmodulin. Nature 388, 882–887.
Mochizuki N, Yamashita S, Kurokawa K, Ohba Y, Nagai T, Miyawaki A, Matsuda M (2001). Spatio-temporal images of growth-factor-induced activation of Ras and Rap1. Nature 411, 1065–1068.
Nagai T, Ibata K, Park ES, Kubota M, Mikoshiba K, Miyawaki A (2002). A variant of yellow fluorescent protein with fast and efficient maturation for cell-biological applications. Nat Biotechnol 20, 87–90.
Nagai T, Yamada S, Tominaga T, Ichikawa M, Miyawaki A (2004). Expanded dynamic range of fluorescent indicators for Ca(2+) by circularly permuted yellow fluorescent proteins. Proc Natl Acad Sci USA 101, 10554–10559.
Nguyen AW, Daugherty PS (2005). Evolutionary optimization of fluorescent proteins for intracellular FRET. Nat Biotechnol 23, 355–360.
Niwa H, Yamamura K, Miyazaki J (1991). Efficient selection for high-expression transfectants with a novel eukaryotic vector. Gene 108, 193–199.
Obata T, Yaffe MB, Leparc GG, Piro ET, Maegawa H, Kashiwagi A, Kikkawa R, Cantley LC (2000). Peptide and protein library screening defines optimal substrate motifs for AKT/PKB. J Biol Chem 275, 36108–36115.
Ohashi T, Galiacy SD, Briscoe G, Erickson HP (2007). An experimental study of GFP-based FRET, with application to intrinsically unstructured proteins. Protein Sci 16, 1429–1438.
Ouyang M, Sun J, Chien S, Wang Y (2008). Determination of hierarchical relationship of Src and Rac at subcellular locations with FRET biosensors. Proc Natl Acad Sci USA 105, 14353–14358.
Rizzo MA, Springer GH, Granada B, Piston DW (2004). An improved cyan fluorescent protein variant useful for FRET. Nat Biotechnol 22, 445–449.
Roux PP, Ballif BA, Anjum R, Gygi SP, Blenis J (2004). Tumor-promoting phorbol esters and activated Ras inactivate the tuberous sclerosis tumor suppressor complex via p90 ribosomal S6 kinase. Proc Natl Acad Sci USA 101, 13489–13494.
Sato M, Ueda Y, Takagi T, Umezawa Y (2003). Production of PtdInsP3 at endomembranes is triggered by receptor endocytosis. Nat Cell Biol 5, 1016–1022.
Violin JD, Zhang J, Tsien RY, Newton AC (2003). A genetically encoded fluorescent reporter reveals oscillatory phosphorylation by protein kinase C. J Cell Biol 161, 899–909.
Yoshizaki H, Ohba Y, Kurokawa K, Itoh RE, Nakamura T, Mochizuki N, Nagashima K, Matsuda M (2003). Activity of Rho-family GTPases during cell division as visualized with FRET-based probes. J Cell Biol 162, 223–232.
Yusa K, Rad R, Takeda J, Bradley A (2009). Generation of transgene-free induced pluripotent mouse stem cells by the piggyBac transposon. Nat Methods 6, 363–369.
Zacharias DA, Violin JD, Newton AC, Tsien RY (2002). Partitioning of lipid-modified monomeric GFPs into membrane microdomains of live cells. Science 296, 913–916.
Zhang J, Ma Y, Taylor SS, Tsien RY (2001). Genetically encoded reporters of protein kinase A activity reveal impact of substrate tethering. Proc Natl Acad Sci USA 98, 14997–15002.